

FIRST ANNUAL REPORT

NASA Research Grant NAG3-1384

Period of Performance

11/19/92 through 11/18/93

**STABILITY LIMITS AND DYNAMICS
OF NONAXISYMMETRIC
LIQUID BRIDGES**

PREPARED BY:

J. IWAN D. ALEXANDER (Principal Investigator)

ANDY RESNIK

WILLIAM. F. KAUKLER

**Center for Microgravity and Materials Research
The University of Alabama in Huntsville
Huntsville, Alabama 35899**

Dynamics and Statics of Nonaxisymmetric Liquid Bridges
NAG3-1384 1st Annual Report
Period of Performance 11/19/92 - 11/18/93

General

During the first year we concentrated on the design and construction of the experimental apparatus, the design and testing of some of the visualization and data acquisition techniques, worked on the theory of the dynamic stability of axisymmetric bridges and carried out some preliminary experiments. The project summary and objectives are reiterated in *1.*, the status of the experiments is outlined in *2.* and the results and status of our theoretical work and numerical simulation are described in *3.* and in the appendix. Work planned for the 3rd year is discussed in section *4.*

1. Project summary and objectives

This program of theoretical and experimental ground-based and low gravity research is focused on the understanding of the dynamics and stability limits of nonaxisymmetric liquid bridges. There are three basic objectives to the proposed work: First, to determine the stability limits of nonaxisymmetric liquid bridges held between non-coaxially aligned disks, second, to examine the dynamics of nonaxisymmetric bridges and nonaxisymmetric oscillations of initially axisymmetric bridges. Some of these experiments will require a low gravity environment and the ground-based research will culminate in a definitive flight experiment. The third objective is to experimentally investigate the vibration sensitivity of liquid bridges under terrestrial and low gravity conditions.

Motivation

The motivation for the proposed work arises from several areas:

-Axisymmetric liquid bridge stability and dynamics have been the subject of numerous theoretical and experimental investigations, while nonaxisymmetric bridges have received less attention.

- The dynamics of liquid bridges (both axisymmetric and nonaxisymmetric), particularly the breakage of bridges and the sensitivity of bridges to vibration, are of particular importance as far as practical aspects of fluids handling in microgravity is concerned.

-Apart from purely fluid dynamic interests, liquid bridge stability is an important factor in determining the stability of molten liquid zones associated with floating zone crystal growth experiments, as well as model floating zone systems designed to study related thermocapillary flow phenomena.

- Finally, space experiments involving the study of zone vibration and response of liquid bridges to uncontrolled g-jitter are a suitable test of the need for vibration isolation techniques for experiments which will operate using liquid bridge configurations. Whether the bridges are melts or lower temperature liquids, the problem of rupture or breakage in response to spacecraft vibration (or g-jitter) is an important consideration for experiment design (eg., the type of isolation, allowable zone slenderness, etc.)

2. Experimental work

During the first year the Plateau tank and support structure was constructed and the liquid bridge vibration mechanisms and automated bridge injection capability, preliminary visualization and data acquisition were completed. On the experimental side, the focus of our work involved density control of the liquid bath, interfacial tension measurements and preliminary static and dynamic experiments. Progress in each of these areas is described below

2.1 Status of the imaging system

The development of a high quality imaging system for the liquid bridge experiment is progressing well. We have the basic system assembled and ready for use. Optical breadboards are rigidly mounted to the optical table at the correct height, and we have all the mounting hardware for the optical components, i.e. optical rail, rail mounts, x-y translational stages, rotational stages, etc. We are in communication with several optical companies who can supply the needed lenses, mirrors, optical flats and pinholes to complete the arrangement.

The imaging system will be, initially, a Fourier transform imager. Plane waves will pass through the tank and bridge, and the light will then be collected and focused to a focal plane. At the focal plane, the image is the Fourier transform of the object. A dc filter will be placed in the center of the plane to allow only the high frequency components to pass. In this way, we can image only the edges of the bridge, which will then be captured using a frame-grabber and analyzed on a computer.

Because the liquid bridge can achieve lengths of up to 4 inches, we require 4 inch optics. In addition, the Fourier transform lenses must be custom made to our specifications, and be as aberration-free as possible. Consequently, most of our resources will go into this piece, as it is the most important and will allow us to accurately determine edge positions and contact angles.

In addition to the transform lenses, we need other lenses for such tasks as producing plane waves, imaging, enlarging, etc. We will acquire additional lenses with various focal lengths and mirrors and optical flats. These will assist us in the fine tuning of the system. Having these tools will also allow us to pursue other methods of imaging, such as interferometry or holography.

2.2 Accuracy of determination of experimental parameters

The important physical parameters are the aspect ratio of the bridge, the liquid volume and the static and dynamic Bond numbers. The liquid volume and the slenderness (aspect ratio) of the bridge depend on the precision with which lengths can be determined. The disk widths are known to within 10 μm . The length of the bridge is set by the positioning device and can be determined with a precision of 1-2 μm . Thus, for bridges of 2.5 cm length the slenderness, $\Lambda = L/2R_0$, can be determined to within $\pm 0.04\%$. Volume can be measured with a precision of 0.1 mm^3 . The accuracy of the volume measurement is about 0.1%. For the Bond number, the main error sources arise in the density and in the determination of surface tension. The surface tension causes the largest error in the Bond number, the density control limits the magnitude of the smallest obtainable Bond number. The liquid bath is a methanol-water solution. Variation of the methanol concentration varies the density difference between the Dow Corning 200[®] silicone oil and the bath. At 83% methanol concentration a condition of neutral bouyancy is obtained. The accuracy of our density measurements is currently 5 parts in 10^4 . If we account for the sources of error

from the density and the surface tension measurements (discussed in the next section) the following lower limits are estimated for the static Bond number B_0 .

R_0 [cm]	B_0
1	$1.9 \times 10^{-2} \pm 7.6 \times 10^{-4}$
0.5	$4.8 \times 10^{-3} \pm 1.9 \times 10^{-4}$
0.25	$1.2 \times 10^{-3} \pm 4.8 \times 10^{-5}$
0.2	$7.6 \times 10^{-4} \pm 3.0 \times 10^{-5}$
0.1	$1.9 \times 10^{-4} \pm 7.6 \times 10^{-6}$

2.3 *Determination of the interfacial tension between silicone fluid and an isopycnic methanol-water solution*

2.3.1. *Introduction*

Our investigations into the dynamical behavior of liquid bridges has prompted us to more precisely determine the interfacial tension between a silicone fluid (polydimethylsiloxane polymer, Dow Corning 200[®] fluid, 100 cs) and a neutrally buoyant solution of methanol in water. Cylindrical liquid bridges, held between rigid supports, are characterized by three parameters: the volume, the aspect ratio r/L , where r is the radius and L is the length of the bridge, and the Bond number $B = \Delta\rho r^2/\gamma$, where $\Delta\rho$ is the density difference between the bridge and the surrounding medium and γ is the interfacial tension. Accurate knowledge of these parameters is crucial for our study of stability limits. Our experimental setup allows for precise determinations of both volume and aspect ratio, but the Bond number, perhaps the most important parameter, is the most difficult to determine accurately. There are two reasons for this. The first concerns precise control of the density of the bridge and the surrounding liquid bath. The second is the difficulty in accurately determining the interfacial tension between the two liquids. Density control is discussed in the previous section. Interfacial tension measurements are outlined below.

2.3.2 *Interfacial tension measurements*

A variety of techniques are available for surface tension measurements which vary in both accuracy and complexity [1]. Most methods involve a relationship between shapes of drops or surfaces and the interfacial tension and involve empirically determined correction factors that may only apply to specific materials. We chose the drop weight technique since it gives accurate results with a minimum of equipment. As a check we also made some measurements using the pendant, or hanging drop method.

The drop weight method [1] is perhaps the simplest method to carry out in a laboratory. Tate's law [1] is used: $W = 2\pi r \gamma f$, where f is a correction factor that allows for the fact that not all the drop will detach from the dropping tip. The correction factor f is a function of tip radius divided by drop radius, or, since the volume is more conveniently measured, $V^{1/3}$. In our case W , the weight of the drop, was $\Delta\rho V$. Correction factors for mercury in air were given by Wilkinson and Aronson [2].

The pendant drop technique is slightly more complex, but still requires a minimum of apparatus. In this case, a static hanging drop was photographed and shape parameters directly measured from the picture. Instead of computer fitting to the entire shape, we used correction factors given by Andreas et al [3] and Adamson [4]. In this case the surface tension is given by

$\gamma = \Delta\rho g(de)^2/H$, where de is the equatorial diameter and H is the correction factor, a function of ds/de . (see Fig. 1) .

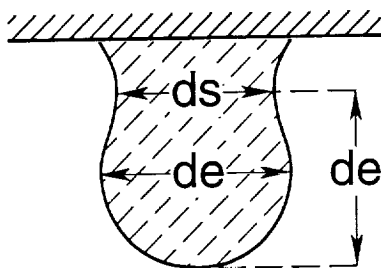


Fig. 1 Schematic of the hanging drop showing the geometrical parameters ds and de .

Provided that the densities of the bridge and bath liquids are sufficiently different, these methods provide accurate data. However, as neutral buoyancy is approached, the volume of the drop increases without bound, unless one assumes (incorrectly) that the surface tension goes to zero as well. However, data taken at other methanol-water concentrations (densities) allow us to interpolate the data through the neutrally buoyant region. If neither of these methods should work, we would be forced to pursue other methods of measuring the interfacial tension, such as the Wilhelmy plate method or a capillary wave method. Both of these place stringent requirements on the experimenter, as both are sensitive measuring procedures, requiring fairly complex apparatus. The Wilhelmy plate method measures the weight of a liquid film on a small object, and thus requires an electrobalance. Capillary wave measurements involve measuring surface deviations on the order of a micron, and would require a sophisticated optical system.

2.3.3 Materials

The silicone fluid was supplied by Dow Corning. It is a bulk polymerized polydimethylsiloxane, with a specific gravity of 0.964 at 25 degrees Celsius. The measured density of the silicone fluid at 23 degrees Celsius was 0.959. Dow Corning gives the surface tension in air at 25 degrees of 20.9 dyne cm^{-1} . The silicone fluid contains not more than 0.5% volatile materials. Methanol supplied by Fisher Chemica was certified to be acetone free, with not more than 0.02% water content. The density was measured and found to be 0.786 at 23 degrees. The water was filtered using Millipore RO[®] system coupled with a Milli-Q[®] deionizer. This allowed us to produce biological grade type I water with a measured density of 0.996 at 23 degrees. The water and methanol were mixed in various proportions and used as different density bath liquids.

Apparatus

The dropping tip was a 20 gauge needle with the end cut square to the sides. Hole integrity was ensured by inserting a wire into the hole at the time of cutting to prevent distortion. Injection was achieved manually using a syringe controlled by a screw drive. By turning a long threaded rod, fluid is injected through plastic tubing into the needle. The syringe, tubing and needle were connected with Luer Lock[®]. The needle was anchored in place by a clamp that was attached to a sturdy base to eliminate unwanted movement or vibration. With careful manipulation, dropping times of up to 5 minutes could be achieved, ensuring maximum drop weight. Although no

temperature control device was used, ambient temperature variation was small enough to ensure that the interfacial tension did not vary appreciably over the time of the experiment.

Procedure

For the drop weight technique, similar procedures were used for situations when the silicone was heavier or lighter than the solution. First, a 100 g solution of methanol and water was prepared by weight percent using an electronic scale with an accuracy of 0.1 mg. This yielded a solution accurate to 0.001%. The receptacle, a square cuvette, was first thoroughly washed with Tergazyme[®] detergent, followed by biological grade-I water, and finally with acetone. The cuvette was allowed to sit until all the rinsing fluids had evaporated. The cuvette was then filled and covered with a cap. The cap contains a small hole through which the needle was inserted. The evaporation rate of the solution was measured over a 3 minute interval. The dropping tip was aligned by eye. (Error analysis has shown that even for a 5 degree misalignment negligible error is introduced in the weight of the drop.) The needle was lowered into the solution and several drops were formed and weighed. The elapsed time was noted, and evaporation rates were accounted for in the final determination of the weight. This procedure was repeated several times. Depending on the relative density between the fluid and the aqueous solution, either silicone fluid or solution was injected into the container. For methanol-water injection, the syringe and tubing were emptied, the apparatus was filled with a new solution that was then expelled as waste. Then, more solution was introduced into the system. In either case, the injected liquid did not wet the tip of the needle, as verified in photographs taken for pendant drop data. The pictures were taken using a standard 35 mm manual camera. Image distortion was checked by imaging a grid, and was found to be zero over the field of view occupied by the drop. Enlargements were made, with end magnifications on the order of 40x. Shape parameters were measured, and the interfacial tension calculated.

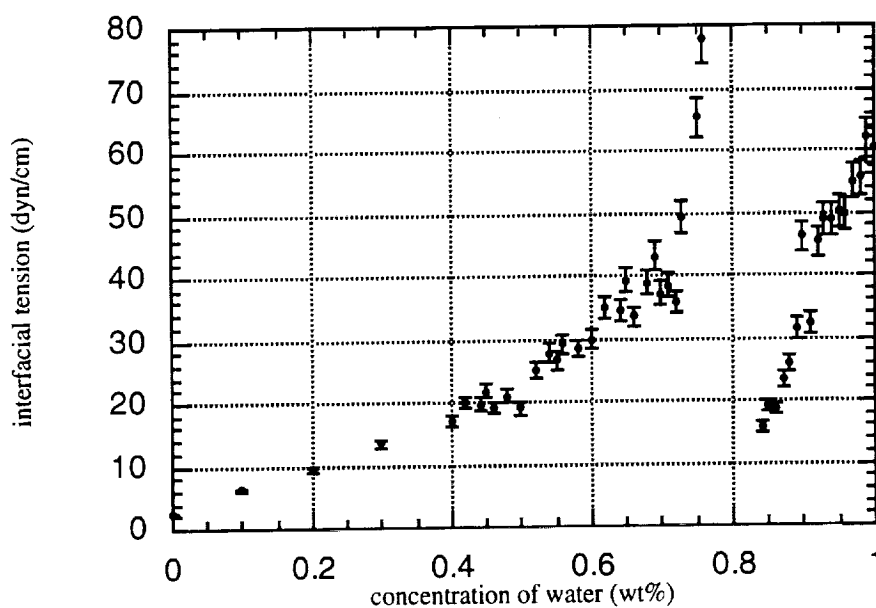


Fig. 2

As a check, the two methods were performed on pure silicone fluid in air. Both methods agreed well with previous data. The pendant drop method tended to give a lower value of the surface tension, while the drop weight method gave a slightly higher value. For silicone oil in air, the hanging drop methods gave a surface tension value of 18.06 ± 0.5434 dyne cm^{-1} for different measurements of the same drop, and 17.17 ± 0.392 dyne cm^{-1} for measurements of different drops. The drop weight method gives 21.29 ± 0.330 dyne cm^{-1} for measurements of different drops, and there is negligible error due to angular displacement. The needle tip was cut square to within 2 degrees. The measured eccentricities of the inner and outer needle diameters were zero and 0.011 ± 0.0073 , respectively. The inner diameter is important for drops in solution, and the outer diameter is important for drops in air. Error as a result from drop-to-drop variations is 2.3%, and error due to measurement of a single drop is 3%.

2.3.5 Results

The results of our measurements are shown in Fig. 2. The surface tension of the silicone fluid in solution ranges from a low of 2.645 dyne cm^{-1} (100% methanol) to a high of 60.48 dyne cm^{-1} (100% water). In addition, the data diverges around the neutrally buoyant point (83% water by weight). As mentioned earlier, this occurs because the relative density passes through zero as the methanol concentration passes through 83%. Approaching neutral buoyancy, the drop size increased exponentially, with a corresponding increase in drop time. The extrema, those closest to the neutral buoyancy condition, correspond to drop volumes on the order of 10 cm^3 . Most data points were taken using only the drop weight method. However, pendant drops were measured at various concentrations (0%, 50% and 100% water), and the values matched those given by the drop weight method, agreeing to within 7%. A cubic fit to the data gives the interfacial tension at neutral buoyancy of 25.7 dyn cm^{-1} .

2.3.6 References

- [1] T.Tate, *Phil.Mag.* **27** 176 (1864).
- [2] M.C. Wilkinson and M.P. Aronson, *Applicability of the Drop-Weight Technique to the Determination of the Surface Tensions of Liquid Metals*, *J. Chem. Soc., Faraday Trans., I*, **69**, 474 (1973).
- [3] J.M. Andreas, E.A. Hauser, and W.B. Tucker, *Boundary Tension by Pendant Drops*, *J. Phys. Chem.*, **42**, 1001 (1938)
- [4] Arthur W. Adamson, *Physical Chemistry of Surfaces*, 5th ed., Wiley and Sons, 31 (1990).

2.4 Preliminary experiments

Experiments in progress or planned for the immediate future involve

- a) a study of the static stability of axisymmetric bridges subject to nonaxisymmetric perturbations
- b) a study of the static stability of bridges held between non-coaxially aligned disks
- c) a study of the dynamic stability of axisymmetric and nonaxisymmetric bridges.

Figures 2- 6 show examples of some preliminary results for static and dynamic conditions. In all cases the images have been grabbed from a video. The half illumination in the background shows a dark background to the left of the bridge. The left side of the bridge is bright and shows a distorted view of the square background grid. The right side of the bridge is dark and its boundary contrasts with the bright background. The breaking of a static bridge is shown in Fig.2. The distance between the supporting disks is 2.525 cm and the diameter is 1 cm. Note the long drawn out neck prior to breaking and the satellite bubble that remains following the breakup. Figure 3

shows a laterally oscillating bridge. The distance between the supporting disks is 2.525 cm and the diameter is 1 cm. The upper disk moves laterally at 1 Hz with an amplitude 0.25 cm. Figure 4 shows a laterally oscillated bridge. The upper disk moves at 1.5 cm s^{-1} with an amplitude of 0.1 cm. Figure 5 shows a sequence with lateral motion of the upper disk with a frequency of 1 hz and an amplitude of 0.1 cm. Note the difference in the deformation modes depicted in Figs. 4 and 5. Figure 6 shows a bridge oscillated laterally at 1 Hz and vertically (both disks) at 1.2 Hz, the bottom disk is rotating at 1rps. Note the excitation of a "c-mode" and its interference with an axisymmetric mode caused by the vertical oscillation.

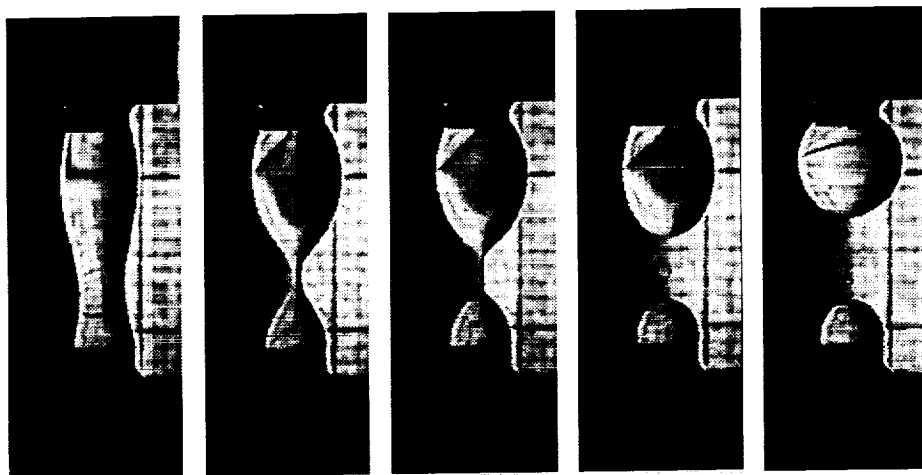


Fig. 3 Breaking of a static bridge

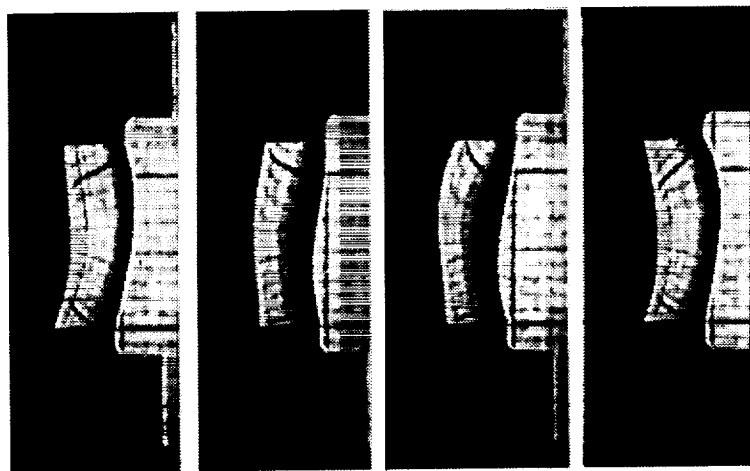


Fig 4. Lateral motion at 1 hz, 0.25 amplitude

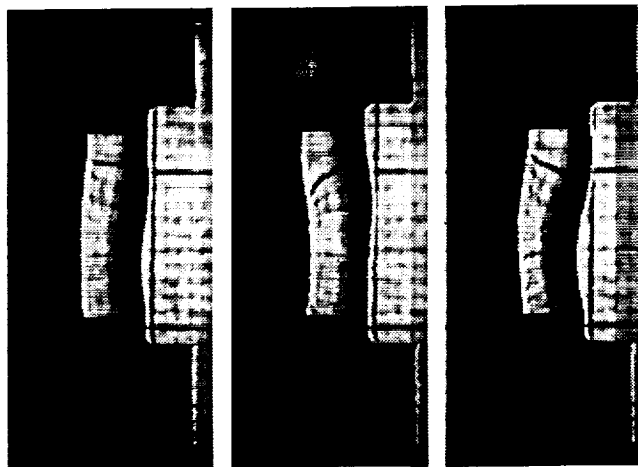


Fig.3 Lateral oscillation at 1 Hz, 0.1 amplitude

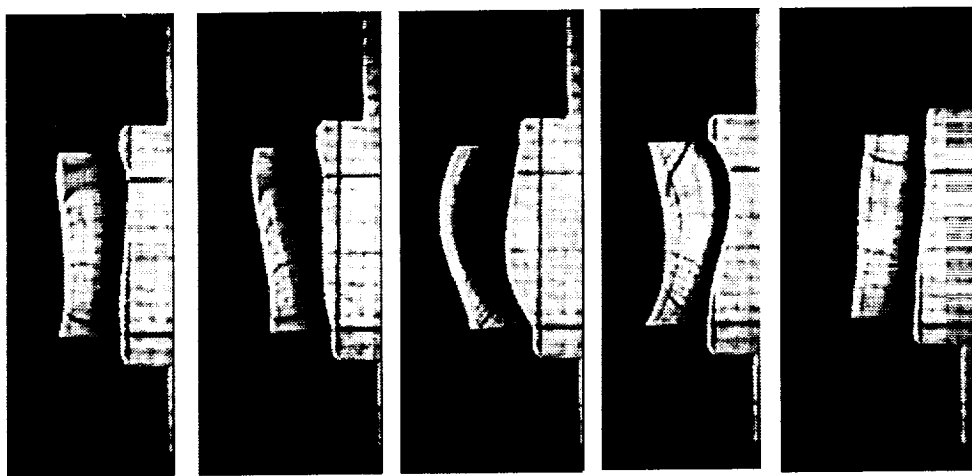


Fig. 4 Rotation (lower disk) at 1 rps, lateral oscillation (upper disk) at 1Hz amplitude 0.4 cm, vertical oscillation (both disks) at 1.2 Hz.

3. Theoretical analysis and numerical simulation

3.1 Dynamic stability of long axisymmetric bridges

This work is part of a joint study carried out at the CMMR and at LAMF in Madrid. The study focuses on the effect of vibration on the stability limits of bridges and how vibration modifies the static stability boundaries. Work has been carried out using a nonlinear model equation for liquid bridges proposed by Rivas and Meseguer (see reference [5] of the appendix). The equation has the form of Duffing's equation with external forcing. In parallel we have been using the 1D-model of Zhang and Alexander [1]. Both models are in good qualitative agreement for the parameter range investigated so far. The results of the study indicate that depending on the nature of the axial vibration the bridge may be stabilized or destabilized relative to the static stability margin. A preprint of a paper describing the results of our study submitted to *Microgravity Science and Technology* is appended to this report.

3.2 Numerical simulation

Work has started on a 3D code, a 2D axisymmetric code is already available. The solution method involves centered finite differences in the radial and axial coordinate directions and a Fourier spectral decomposition in the azimuthal direction. The incompressible Navier-Stokes equations are solved in primitive variable form. For an M-term Fourier approximation this yields M non-linear partial differential equations with r and z as independent variables. The M equations for the pressure and velocity are solved using and an ADI scheme [2]. A pressure correction equation is used to obtain the pressure. This is solved using a conjugate gradient squared technique.

For the primitive formulation the solution procedure (which we have used successfully for axisymmetric steady and time-dependent computation [3,4]) is as follows: A nonorthogonal coordinate transformation,

$$\eta = z, \quad \xi = \frac{r}{R(\theta, z, t)},$$

allows an irregular free boundary to coincide with a cylindrical coordinate line (or surface) without the need to solve a coupled set of Laplace equations [5,6]. The resulting equations are discretized following a semi-implicit difference scheme. The conditions for force balance tangent to the surface and kinematic condition at the free surface are solved along with the Navier-Stokes and continuity equations. The condition for the force balance normal to the surface is used to determine the free surface shape. In addition, an "outer" iterative procedure is needed to locate the free surface.

The unsteady free boundary problem for a cylindrical liquid zone is solved as follows. The initial conditions correspond to either zero or finite steady residual acceleration situations. For the unsteady calculation the solution scheme is similar to that used by Kang and Leal [5] and Ryskin and Leal [6]. The following iterative procedure is adopted:

1. guess the free surface shape for the new timestep;
2. obtain the approximate pressure and velocity fields by transforming the governing equations and boundary conditions to a circular cylindrical domain via a nonorthogonal transformation and solve them using the scheme outlined above;
3. use the normal force balance condition at the free surface to decide how to update the free surface location;
4. return to step 2. Repeat until convergence is obtained by satisfying all equations and boundary conditions to a specified degree of accuracy for this timestep.

We are currently testing the code and anticipate being able to apply the code to nonaxisymmetric bridge vibration problems soon.

3.3 References

- [1] Y.Q. Zhang and J.I.D. Alexander, Sensitivity of Liquid Bridges to Axial Vibration, *Physics of Fluids*, A 2 (1990) 1966-1974.
- [2] D.W. Peaceman and H.H. Rachford, *J. SIAM*, 3 (1955) 28-41.
- [3] Y.-Q. Zhang., and J.I.D. Alexander, The sensitivity of a nonisothermal liquid bridge to residual acceleration, *Microgr. Sci. Tech. IV* (1991) 128-129; and the Proceedings of the IUTAM Symposium on Microgravity Fluid Mechanics, Bremen, 1991.

- [4] Y.-Q. Zhang., and J.I.D. Alexander, Surface tension and buoyancy-driven flow in a nonisothermal liquid bridge, *Int. J. Num. Meth. Fluids*, 14 (1992) 197-216.
- [5] I.S. Kang Numerical solution of axisymmetric unsteady free-boundary problems in a uniaxial straining flow, *Phys. Fluids*, 30 (1987) 1929-1940.
- [6] G. Ryskin and L.G. Leal, Numerical solution of free boundary problems in fluid mechanics. Part 1. The finite difference technique., *J. Fluid Mech.*, 148 (1984) 1-17.

4. Work planned for the second year

During the second year we plan to complete the study of nonaxisymmetric breaking of axisymmetric bridges under static and dynamic conditions, a study of the static stability of bridges held between noncoaxially aligned disks and to have started a study of the lateral vibration of bridges.

5. Appendix (Submitted to Microgravity Science and Technology, 1993)

DYNAMIC STABILITY OF LONG AXISYMMETRIC LIQUID BRIDGES

J. Meseguer, M.A. González and J.I.D. Alexander

This paper deals with the non-linear forced oscillations of axisymmetric long liquid bridges held between equidimensional disks. The dynamics of the liquid bridge has been analyzed by using a self-similar, one dimensional model. The influence of the dynamics on the static stability limits, as well as the main characteristics of the non-linear behaviour of long liquid bridges, have been studied within the range of validity of the mathematical model used here.

Prof. J. Meseguer, M.A. González: Lamf, E.T.S.I. Aeronáuticos, Universidad Politécnica de Madrid, 28040 Madrid, Spain.

Dr. J.I.D. Alexander: Center for Microgravity and Materials Research (CMMR), The University of Alabama in Huntsville, Huntsville, Alabama 35899, USA.

1. INTRODUCTION

For some time, isothermal liquid bridges have attracted the attention of many investigators and a large number of published papers on this topic have resulted (a review of the literature related to liquid bridges can be found in *Sanz-Andres* [1]). Because of the number of parameters involved, the study of liquid bridges has been a formidable task which extends since the early work of *Gillette & Dyson* [2] to the recent paper of *Slobozhanin & Perales* [3]. Most of these papers are only concerned with static stability limits. As far as we know, only a few attempts have been made to analyze the influence of the dynamics of the liquid bridge, and these efforts have been centered more in the dynamics itself than in its influence on the stability limits (*Meseguer* [4], *Rivas & Meseguer* [5], *Perales & Meseguer* [6], *Sanz & López-Díez* [7], *Zhang & Alexander* [8], *Langbein* [9], *Schulkes* [10], among others).

In this paper the influence of the dynamics on the stability limits of liquid bridges is analyzed by using a simplified one-dimensional, self-similar model which, in spite of its simplicity, allows us to get some feeling about the dynamical behaviour of long liquid bridges. Associated with stability limits is the concept of a stability margin. This has been defined as the difference between the energy of the stable equilibrium shape and the energy of unstable shape for a given liquid bridge. The stability margin yields an estimate of the minimum energy needed to break a liquid bridge through a given perturbation. Stability margins are discussed in Section 2, in Section 3 the forced oscillations of long liquid bridges are analyzed, and stability diagrams for such perturbations are obtained.

2. PROBLEM FORMULATION

The fluid configuration under consideration consists of an axisymmetric liquid bridge, with constant density ρ , kinematic viscosity ν and surface tension σ . It is held by capillary forces between two coaxial, solid disks of radius R which are a distance L apart, as sketched in Fig. 1.

The volume of liquid, V , is assumed to be almost the volume of a cylinder of the same R and L , $V \approx \pi R^2 L$, and it is also assumed that there is a small acceleration acting parallel to the liquid bridge axis. To describe the behaviour of such a fluid configuration the following dimensionless parameters are introduced: slenderness $\Lambda = L/2R$, dimensionless volume $V = V/R^3$, Bond number $B = \rho g R^2 / \sigma$ and viscosity parameter $C = \nu(\rho/\sigma R)^{1/2}$. In addition to these parameters, it must be stated that all physical magnitudes used in the following have been made dimensionless by using R and $(\rho R^3/\sigma)^{1/2}$ as characteristic length and characteristic time, respectively.

It has been demonstrated in *Rivas & Meseguer* [5] that near the static stability limit of cylindrical liquid bridges ($\Lambda = \pi$, $B \approx 0$, $V \approx 2\pi\Lambda$) there is a self-similar solution for the dynamics of the liquid bridge. These authors performed their analysis by using a one-dimensional model in which the axial velocity is assumed to be dependent on the axial coordinate z and the time t , but not on the radial coordinate r . (This hypothesis has is valid provided the slenderness is large enough, say $\Lambda > 1.5$, *Perales & Meseguer* [6]). Within the validity range of such analysis the variation with time of the interface deformation is given by the Duffing equation

$$\alpha_{\theta\theta} + \gamma\alpha_{\theta} - m\alpha - \alpha^3 = \tilde{\beta} \quad (1)$$

where

$$\alpha = \frac{1}{4} A \left(\frac{1}{3}\delta\right)^{-1/2}, \quad \theta = \frac{2}{5} t (2\delta)^{1/2}, \quad \gamma = \frac{5}{2} C (2\delta)^{-1/2}, \quad \tilde{\beta} = \frac{1}{2} B \left(\frac{1}{3}\delta^3\right)^{-1/2}, \quad (2)$$

are the self-similar variables and parameters. Here A is the amplitude of the interface deformation, which in this model varies as $S(z,t) = 1 + A(t)\sin\pi z/\Lambda$. Formally A measures the deformation of a magnitude proportional to the liquid bridge cross-section since $S = F^2$. The parameter δ is a reduced slenderness which includes volume effects: $m\delta = 1 - \frac{\Lambda}{\pi} + \frac{1}{2} \left(\frac{V}{2\pi\Lambda} - 1\right)$, where δ is positive and m takes account for the sign ($m = \pm 1$); t is the dimensionless time and the parameters C and B have been already defined.

To simplify the explanation, let us assign the self-similar variables and parameters involved in the problem, as defined by expressions (2), labels indicating their main physical meaning. Thus, in the following we refer to α , θ , γ and $\tilde{\beta}$ as deformation of the liquid bridge interface, time, viscosity and Bond number, respectively. Let us also assume that gravity oscillates around some mean value, in such a way that in self-similar variables the variation with time of Bond number can be written as, $\tilde{\beta} = \beta + b\cos\Omega\theta$, where Ω stands for the self-similar frequency of the imposed perturbation. In such case eq. (1) would be

$$\alpha_{\theta\theta} + \gamma\alpha_{\theta} - m\alpha - \alpha^3 = \beta + b \cos \Omega\theta \quad (3)$$

which allows one to analyze, within the validity range of this model, both the static stability margin and the forced non-linear response of the liquid bridge.

The static stability margin results from eq. (3) with $b = 0$. The potential energy of the liquid bridge, which accounts for both gravity field and surface energies, in self-similar variables will be

$$\xi = -\frac{1}{2}m\alpha^2 - \frac{1}{4}\alpha^4 - \beta\alpha \quad (4)$$

where ξ is related to dimensionless energy (made dimensionless with σR^2) through the expression

$$\xi = \frac{16}{3}(\pi\delta)^{-2}(E - E_0) \quad (5)$$

E_0 accounting for all terms contributing to energy which do not depend on the interface deformation. Equilibrium shapes are given by

$$\frac{d\xi}{d\alpha} = -m\alpha - \alpha^3 - \beta = 0 \quad (6)$$

Eq. (6) has one real root if $m = +1$, which is unstable ($d^2\xi/d\alpha^2 < 0$), and three real roots, $\alpha_1 > \alpha_2 > \alpha_3$, in the case $m = -1$. From these, the two extreme roots, α_1 and α_3 , correspond to unstable equilibrium shapes, whereas the central one represents a stable configuration. Thus, within this approximation the stability margin will be the difference between the energy of the unstable equilibrium shapes and of the stable one, $\Delta\xi = \xi_{unstable} - \xi_{stable}$. This behaviour is summarized in Fig. 2, where the variation of the roots α_1 , α_2 and α_3 with β as well as the stability margins $\Delta\xi_3 = \xi(\alpha_3) - \xi(\alpha_2)$ and $\Delta\xi_1 = \xi(\alpha_1) - \xi(\alpha_2)$, are shown. Obviously, the stability margin is defined by the smaller of such values, $\Delta\xi_1$ in our case. In the following we will denote this as $\Delta\xi$. According to Eq. (5), in dimensionless variables the stability margin is given by $\Delta E = \frac{3}{16}\pi^2\Delta\xi\delta^2$, that is, the stability margin is proportional to the square of the distance to the stability limit (the stability limit being $\delta = 0$), the proportionality constant, $\Delta\xi$, being smaller as the Bond number increases. This factor, and hence the stability margin, becomes zero when $\beta = 2\sqrt{3}/9$. In dimensionless variables this represents the variation with Bond number of the stability limit of almost cylindrical liquid bridges, $B = \frac{4}{9}\delta^{3/2}$, previously calculated by *Vega & Perales* [11].

3. DYNAMIC STABILITY

The stability margin, or safety margin, represents a limit to the minimum energy needed to break the liquid bridge. That means that, for a given perturbation, the response of the liquid bridge will depend on the energy of the perturbation; the liquid bridge will remain stable if the energy is smaller than the corresponding stability margin and it could be unstable if such energy becomes bigger. Of course in this last case the evolution of the liquid bridge depends on how the perturbation is imposed and on how such energy is dissipated because of viscosity. To fix our ideas let us consider the forced oscillation of the liquid bridge in gravitationless conditions ($\beta = 0$, $b \neq 0$). In that case $\alpha_2 = 0$ and $\alpha_1 = -\alpha_3 = 1$, so that $\Delta\xi = 1/4$. The time variation of the interface is now defined by the expression

$$\alpha_{\theta\theta} + \gamma\alpha_{\theta} + \alpha - \alpha^3 = b \cos(\Omega\theta + \varphi) \quad (7)$$

which, assuming steady oscillations are reached, can be integrated in a first approximation [11] obtaining $\alpha = a \cos \Omega\theta$, where a is related to viscosity, γ , to the amplitude of the perturbation, b , and to the frequency of the perturbation, Ω , through the equation

$$a^2 \left(1 - \Omega^2 - \frac{3}{4} a^2 \right)^2 + \gamma^2 \Omega^2 a^2 = b^2 \quad (8)$$

Within this approximation the oscillation of the liquid bridge can be easily visualized by plotting the liquid bridge evolution in the phase space (deformation-velocity-energy diagram), as shown in Fig. 3. Note that, since we are considering an evolution, kinetic energy must be also taken into account, so that at every point of the phase space the energy will be the sum of the potential energy plus the kinetic energy:

$$\xi = \frac{1}{2} \alpha^2 - \frac{1}{4} \alpha^4 + \frac{1}{2} \alpha_{\theta}^2 \quad (9)$$

Two different oscillations of the liquid bridge, with amplitude $a < 1$, have been also represented in Fig. 3. One oscillation corresponds to $\Omega < 1$ and the other to $\Omega > 1$. Note that, for the motion under consideration, the energy of the liquid bridge, and hence the energy of the perturbation, can be greater than that corresponding to the stability margin ($\Delta\xi = 1/4$) and the configuration remains stable, as in the $\Omega > 1$ case.

According to the plot of Fig. 3, the liquid bridge will be unstable when $a = 1$, and, in that case, eq. (8) gives us the relationship between the viscosity γ and the parameters defining the perturbation

$$\gamma^2 = \Omega^{-2} \left[b^2 - \left(\frac{1}{4} - \Omega^2 \right)^2 \right] \quad (10)$$

Once b and Ω are fixed, the liquid bridge evolution will be stable if the viscosity of the liquid is greater than the value resulting from eq. (10), otherwise it will be unstable. This behaviour is summarized in Fig. 4, which has been plotted using eq. (10). For a given viscosity γ and frequency Ω the evolution will be unstable if the point representing this evolution lies on the left of the corresponding b -curve, and stable if the point lies on the right.

Of course, this description of the phenomenon must be regarded as qualitative. The results obtained are based on the assumption that the response of the liquid bridge is co-sinusoidal ($\alpha = a \cos \Omega\theta$) which in some cases is only a rough approximation to the solution of eq. (7).

To get more precise results, equation (7) has been numerically integrated by using a fourth-order Runge-Kutta method and the trajectories in the phase-plane obtained. Depending on the values of the parameters involved (γ , b and Ω) and the initial conditions these trajectories can be closed curves (the deformation of the liquid bridge interface, α , remains bounded no matter what the

value of θ is) or the deformation continuously grows with time. The first case means that the liquid bridge is stable for the imposed perturbation, whereas in the second case the fluid configuration becomes unstable. The border between the two cases being the dynamic stability limit for the perturbation under consideration. When forced oscillations are considered the stability limit depends, as already stated, on the nature of the imposed perturbation and on the initial conditions. To avoid the influence of the initial transient, calculations have been performed as follows: first a set of values of the parameters γ , b and Ω for which the liquid bridge evolution is clearly stable is chosen (this is achieved by selecting a high value of viscosity γ). Once a steady oscillation is reached, the value of one of the parameters is slightly changed (in our case the value of γ is slightly reduced at the beginning of a cycle); in this way initial conditions for the second set of values of the parameters are extremely close to that corresponding to a steady oscillation and transient effects due to initial conditions can be made negligible.

The results obtained are shown in Fig. 5. Also in this plot each one of the curves $b = \text{constant}$ represents the corresponding stability limit. Points on the right of a given curve represent stable evolutions (high values of the viscosity, γ) whereas those of the left side region (low values of γ) corresponds to unstable evolutions. Note that once γ and b are fixed there is one or even two sets of values of Ω for which the liquid bridge evolution becomes unstable.

The response of the liquid bridge, defined as α_m/b where α_m stands for the maximum value of α in each cycle, is shown in Fig. 6 for different values of b .

To assess the importance of initial conditions on the response of the liquid bridge equation (7) has been integrated again with initial conditions $\alpha = 0$, $\alpha_\theta = 0$. The stability limit corresponding to $b = 0.5$ obtained by using this initial conditions (curve labelled 2 in Fig. 7) is compared with the calculated taking “steady” initial conditions (curve 1). Note that the influence of initial conditions becomes negligible when Ω is small enough, but that differences can be remarkable as the value of Ω increases.

Finally, it should be noted that the Duffing equation, used here to analyze the non-linear forced oscillation of long liquid bridges, is a typical example of non-linear oscillator in which chaotic phenomena appear [12]. Such chaotic behaviour has been detected in our calculation when both Ω and γ are small, although no attempts have been made to perform a detailed analysis of such behaviour, which is out of the scope of this paper.

ACKNOWLEDGMENTS

This work has been supported by the Spanish Comisión Interministerial de Ciencia y Tecnología (CICYT) and is part of a more general endeavour for the study of fluid physics and materials processing under microgravity (Project No. ESP92-0001-CP), and through the National Aeronautics and Space Administration through NASA grant NAG8-

REFERENCES

- 1.- Sanz-Andres, A., Static and dynamic response of liquid bridges, in *Microgravity Fluid Mechanics*, Ed. Rath, H.J. (Springer-Verlag, Berlin, 1992), 3-7.
- 2.- Gillette, R.D. & Dyson, R.C., Stability of fluid interfaces of revolution between equal solid circular plates, *Chem. Eng. J.* 2, 44-54 (1971).
- 3.- Slobozhanin, L.A. & Perales, J.M.: Stability of liquid bridges between equal disks in an axial gravity field, *Phys. Fluids A*, in press.
- 4.- Meseguer, J., The breaking of axisymmetric slender liquid bridges, *J. Fluid Mech.* 130, 123-151(1983).
- 5.- Rivas, D. & Meseguer, J., One dimensional, self-similar solution of the dynamics of axisymmetric slender liquid bridges, *J. Fluid Mech.* 138, 417-429 (1984).
- 6.- Perales, J.M. & Meseguer, J., Theoretical and experimental study of the vibration of axisymmetric viscous liquid bridges, *Phys. Fluids A* 4, 1110-1130 (1992).
- 7.- Sanz, A. & López-Díez, J., Non-axisymmetric oscillations of liquid bridges, *J. Fluid Mech.* 205, 503-421(1989).
- 8.- Zhang, Y & Alexander, J.I.D., Sensitivity of liquid bridges subject to axial residual acceleration, *Phys. Fluids A* 2, 1966-1974 (1990).
- 9.- Langbein, D., Oscillations of finite liquid columns, *Microgravity Sci. Technol.* 5, 73-85 (1992)
- 10.- Schulkes, R.M.S.M., Non linear liquid bridge dynamics, in *ESA SP-333, Vol. 1* (ESA Publ. Div., ESTEC, Noordwijk 1992), 61-65.
- 11.- Vega, J.M. & Perales, J.M., Almost cylindrical isorotating liquid bridges for small Bond numbers, in *ESA SP-191*, (ESA Publ. Div., ESTEC, Noordwijk 1992), 247-252.
- 12.- Stoker, J.J., *Nonlinear vibrations, Vol. II* (Interscience, 1966).
- 13.- Thompson, J.M.T. & Steward, M.B., *Nonlinear dynamics and chaos* (John Wiley & Sons Ltd., Chichester, 1988).

FIGURE CAPTIONS

- Fig. 1. Geometry and coordinate system for the liquid bridge problem.
- Fig. 2. Variation with the Bond number, β , of the roots, α_i , of eq. (6), which define the equilibrium shapes of a slender liquid bridge, and variation with β of the difference, $\Delta\xi_i$, between the energy of each one of the unstable equilibrium shapes and of the stable one.
- Fig. 3. Phase space (deformation of the interface, α , velocity, α_θ , and energy, ξ) of the forced oscillations of a liquid bridge according to the simplified model given by eq. (8). There are two evolutions represented in this plot, $\Omega > 1$ and $\Omega < 1$ where Ω stands for the pulsation of the forcing action.
- Fig. 4. Stability diagram in self-similar variables as given by eq. (10). Points on the left of each curve $b = \text{constant}$ are unstable for this value of b , whereas those lying on the right are stable.
- Fig. 5. Stability diagram in self-similar variables obtained by numerical integration of eq. (3). Points on the left of each curve $b = \text{constant}$ are unstable for this value of b , whereas those lying on the right are stable.
- Fig. 6. Variation with the self-similar pulsation Ω of the maximum deformation of the interface, a_m , divided by the intensity of the forcing perturbation, b . Numbers on the curves indicate the value of the viscosity, γ .
- Fig. 7. Influence of the initial conditions on the stability diagram. Curves 1 and 2 have been obtained under different initial conditions as explained in the text.

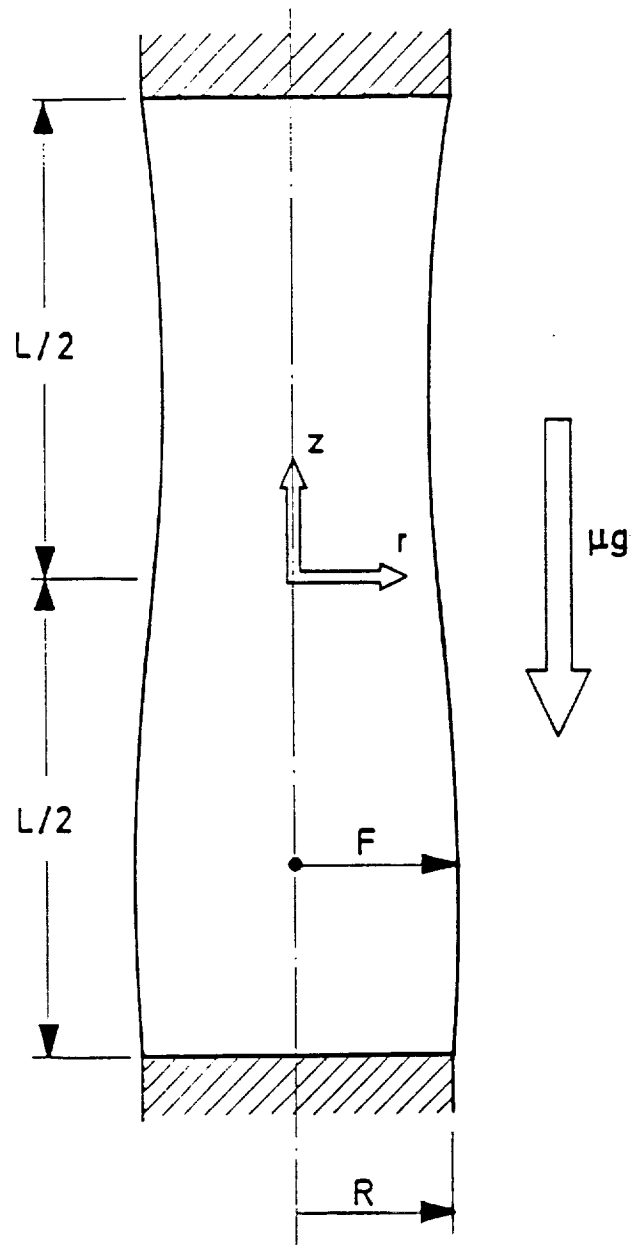


FIG. 1

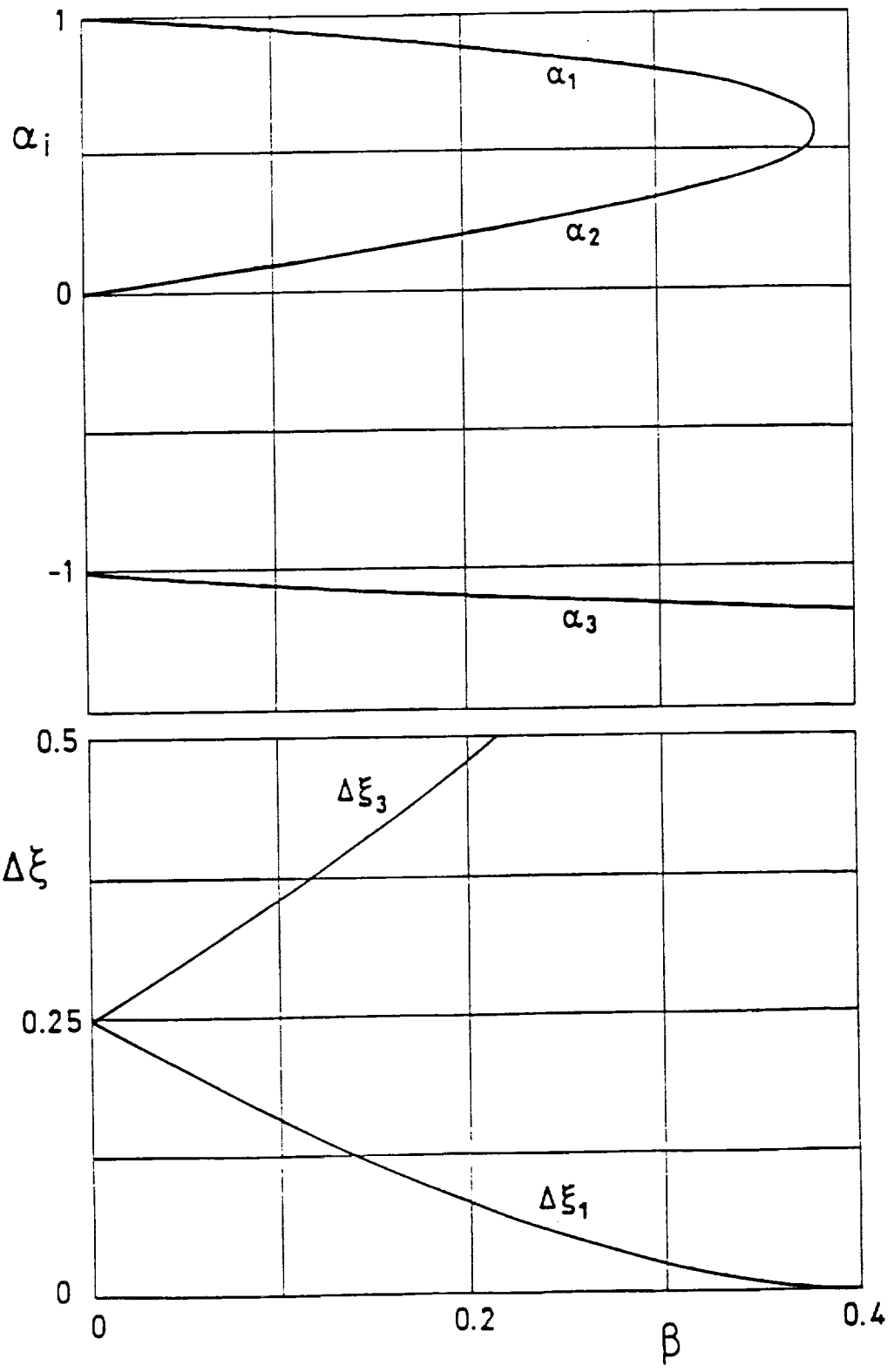


FIG. 2

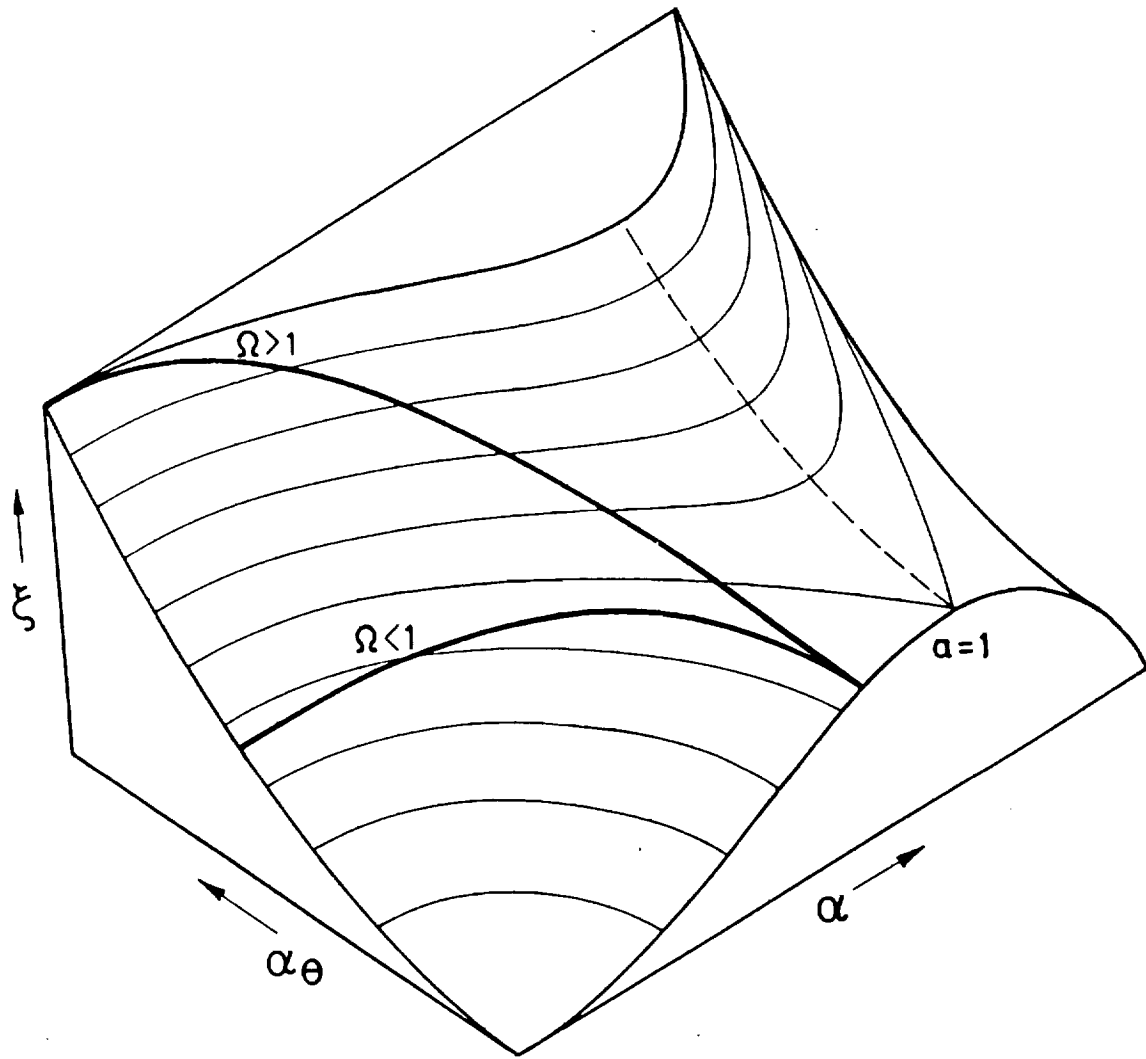


FIG. 3

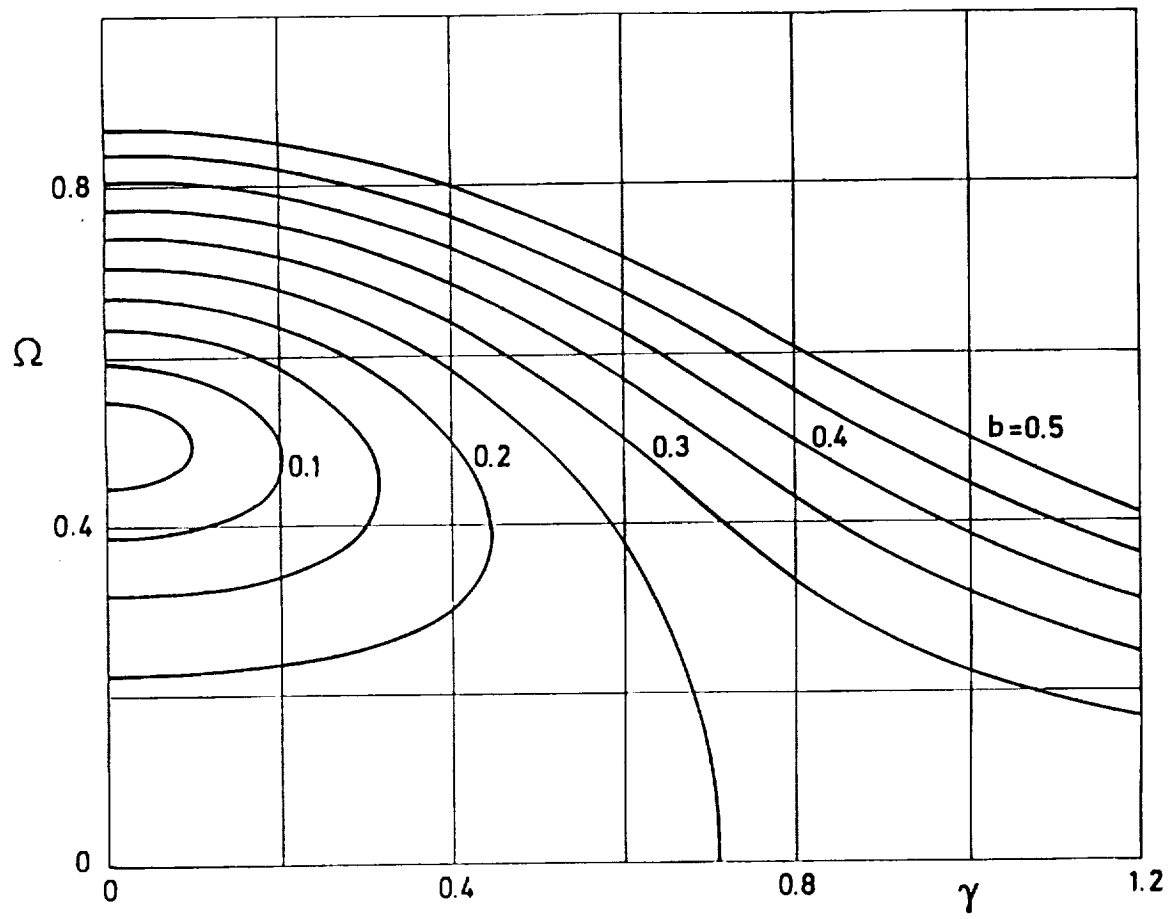


FIG. 4

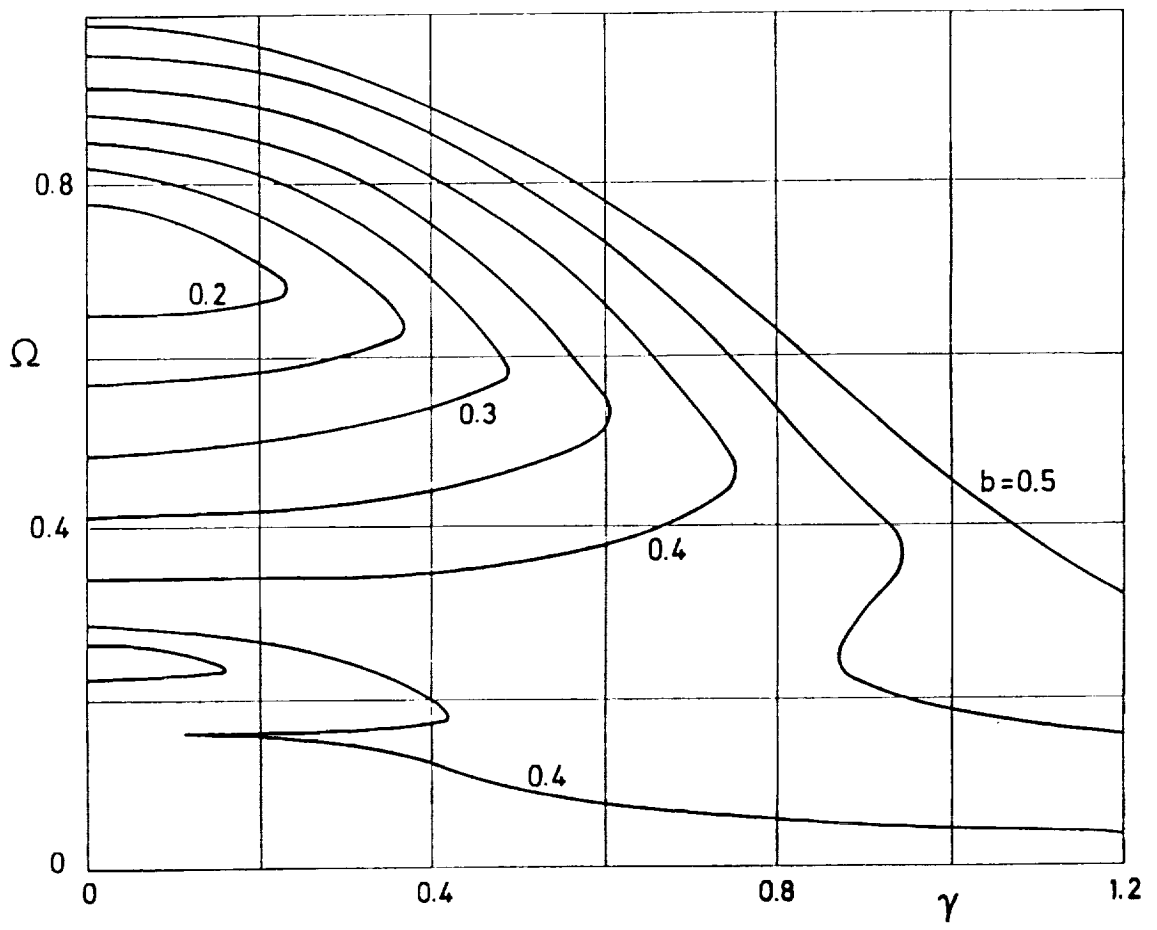


FIG. 5

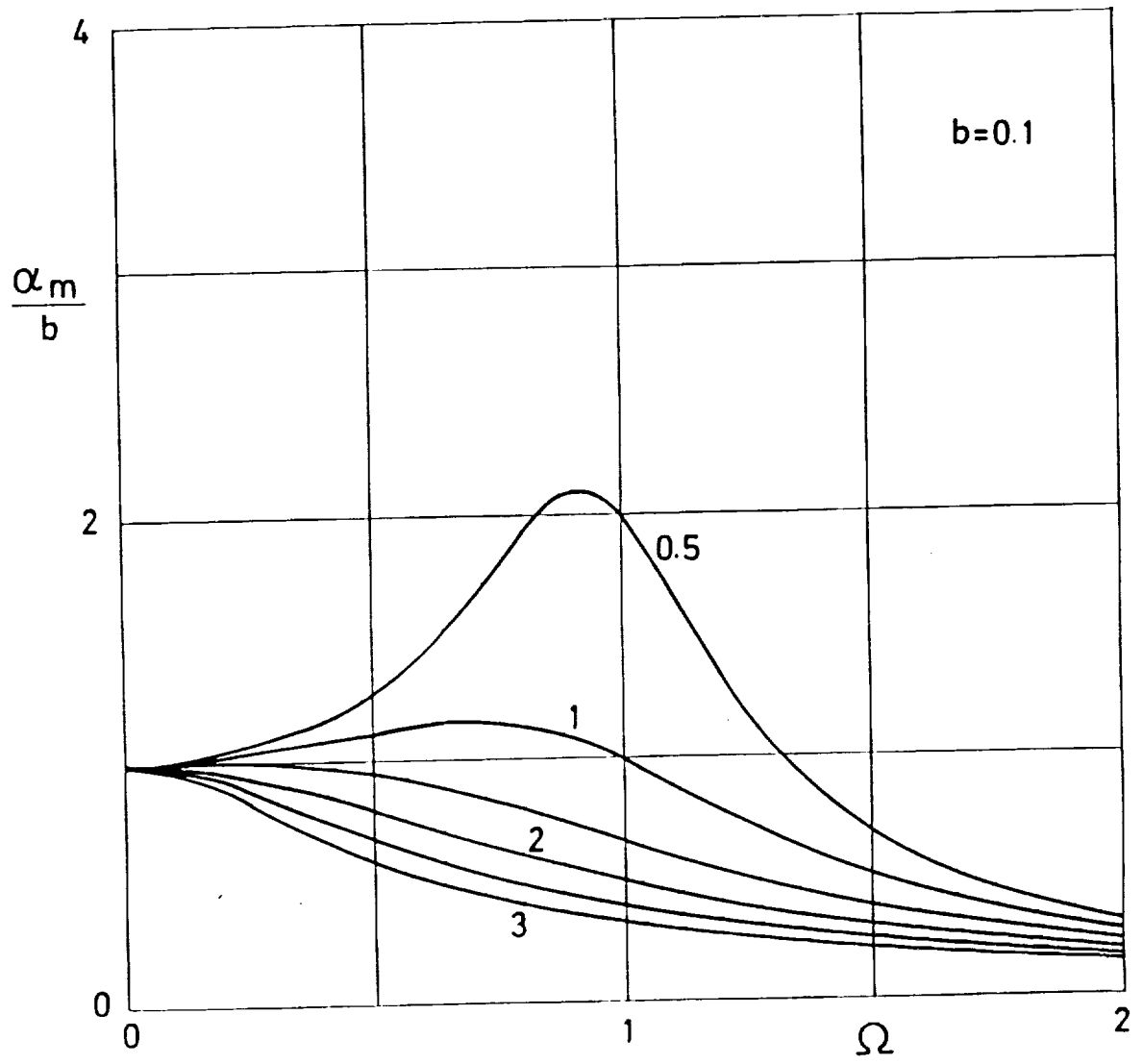


FIG. 6a

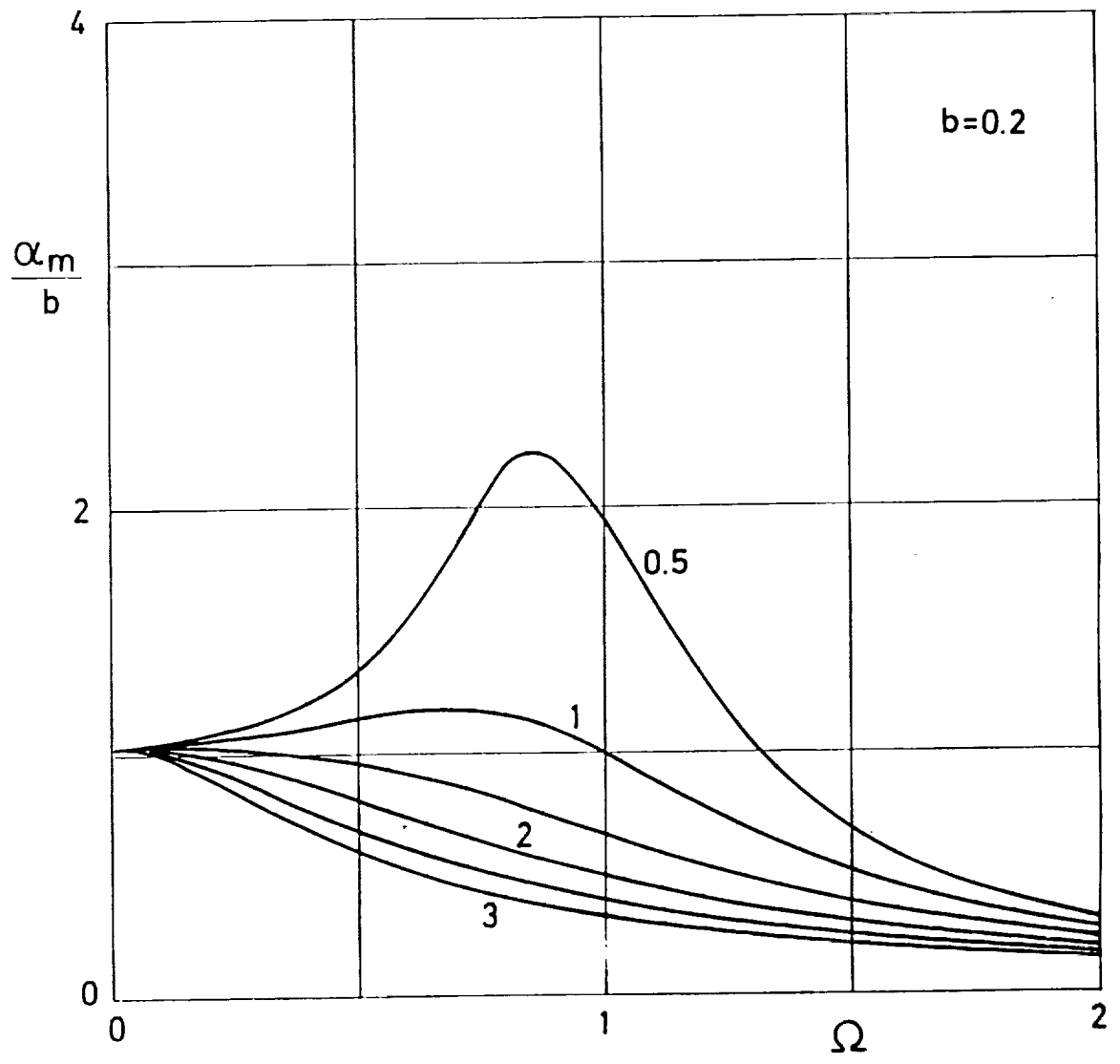


FIG. 6b

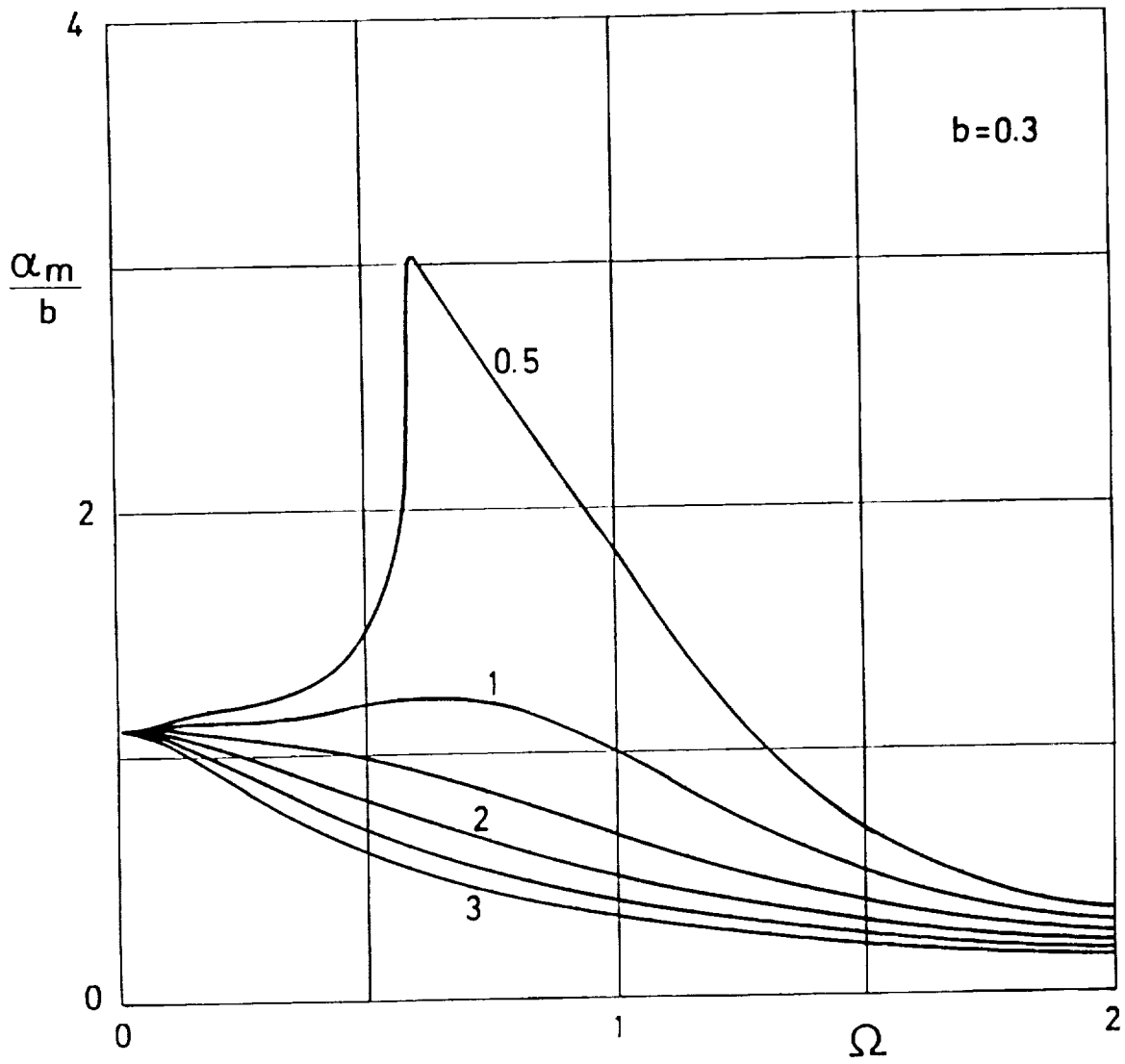


FIG. 6c

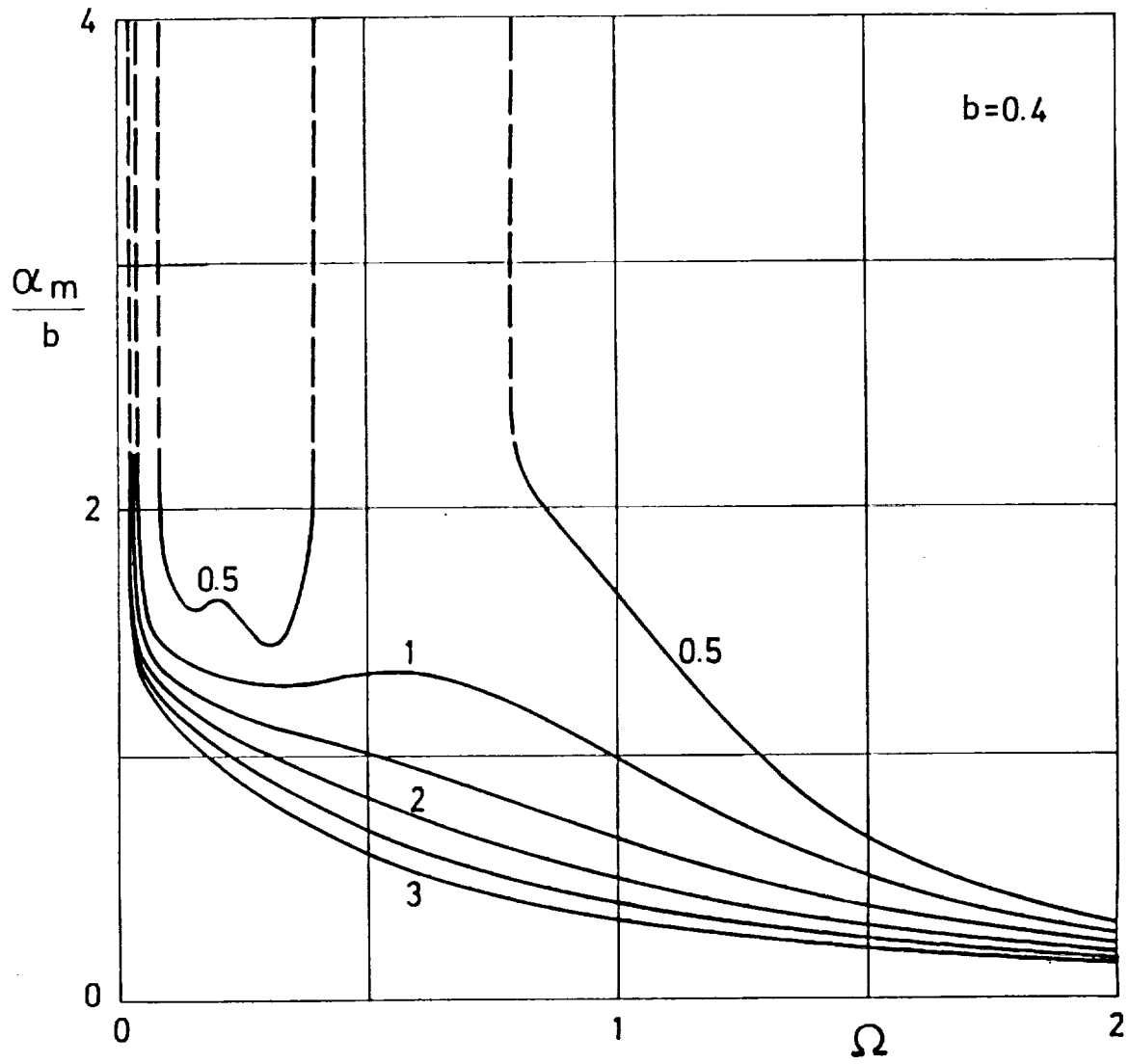


FIG. 6d

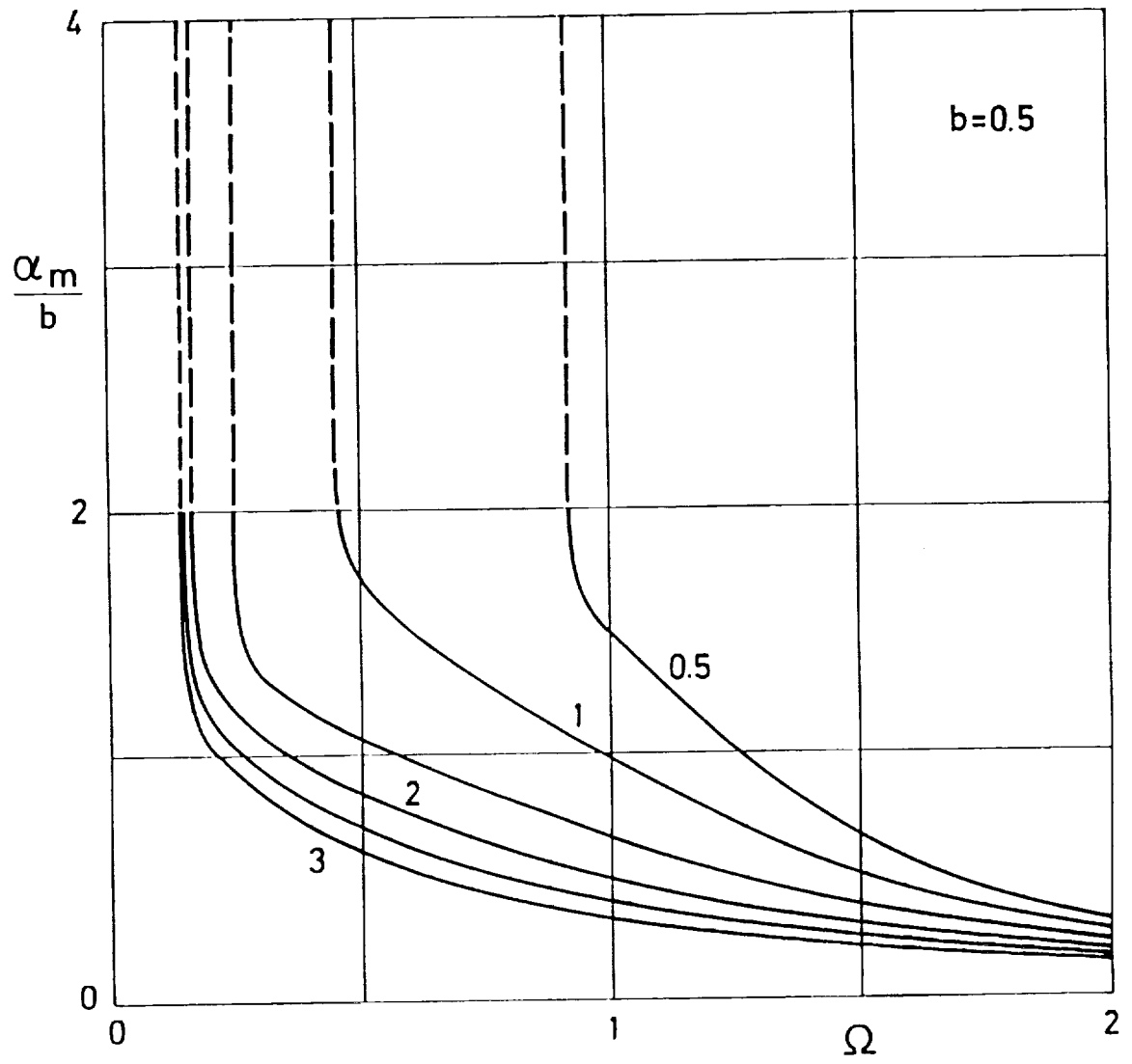


FIG. 6e

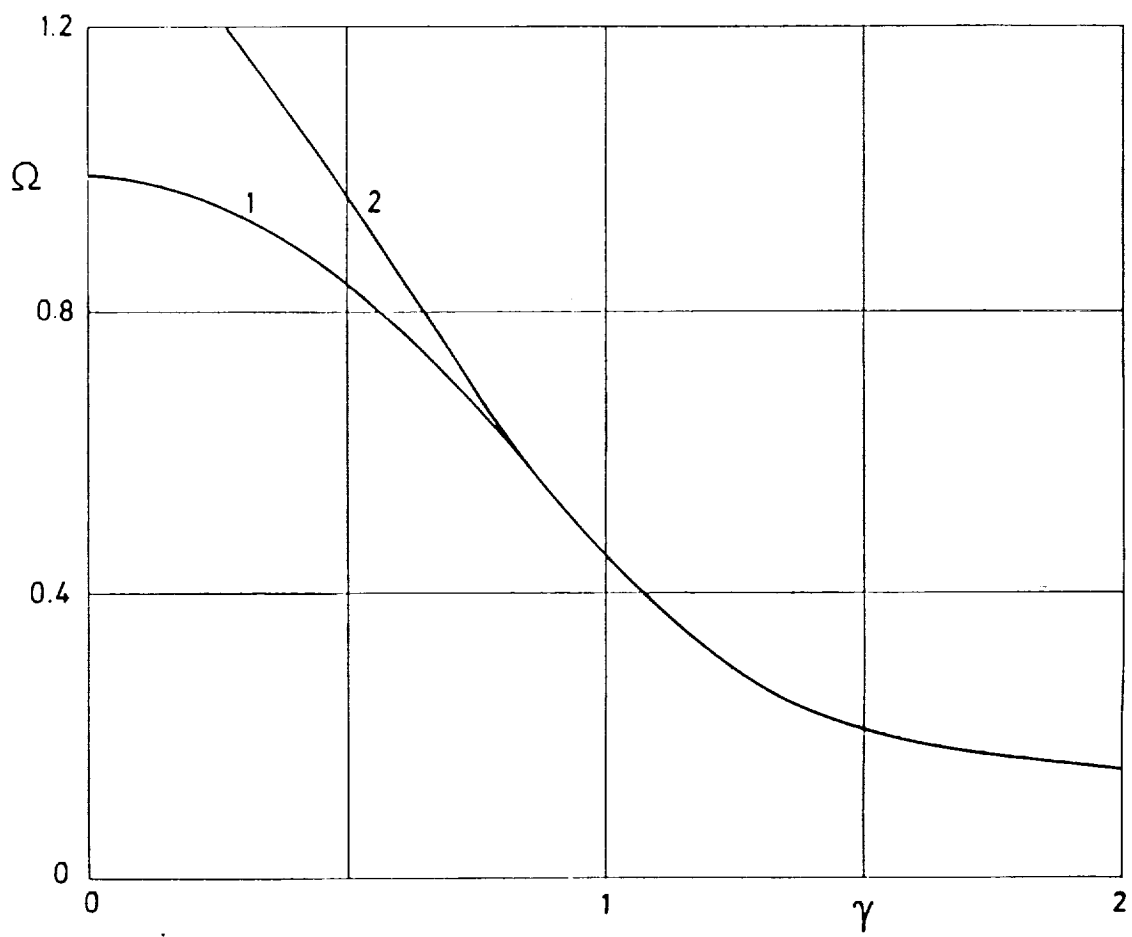


FIG. 7